Meccanica
https://doi.org/10.1007/s11012-024-01883-2

RESEARCH

Discrete macro-models of nonlinear interlocking mechanisms in the out-of-plane failure of masonry walls

B. Pantò · L. Giresini · C. Casapulla

Received: 18 April 2024 / Accepted: 9 September 2024

Abstract Historical unreinforced masonry (URM) constructions are generally vulnerable to out-of-plane (OOP) failures due to the absence of rigid floors and poor connections between orthogonal walls. That leads to the activation of rocking mechanisms of external walls, whose ultimate force and displacement are affected by complex nonlinear interactions with sidewalls. These interactions are often neglected in the engineering practice, potentially leading to significant approximations, as demonstrated by experimental and numerical studies available in the literature. As a novel contribution to the field, this paper presents an upgraded discrete macro-element model (DMEM) to predict the rocking capacity of OOP loaded URM walls interacting with sidewalls. Considering both the onset and the evolution of the rocking mechanism of the front wall, interlocking effects with the sidewalls are first simulated through frictional resistances using the macro-block model (MBM) and the nonlinear kinematic approach of limit analysis. Then, the upgraded DMEM is implemented on the basis of the equivalence between the continuous distribution of these forces, introduced as a further novelty of the paper, and the discrete distribution of lateral elastic-plastic links, accounting for mechanical and geometrical nonlinearities. The results of the two models are discussed in terms of both frictional resistance-displacement and pushover curves, referring to a case study of a front wall belonging to a two-storey URM building. The wall response is also compared with the results derived from the original source of the case study and analysed by changing the number of nonlinear links to define different levels of accuracy.

Keywords Rocking masonry walls · Interlocking effects · Nonlinear kinematic analysis · Pushover analysis · Nonlinear springs · Frictional resistances

1 Introduction

The seismic assessment of existing masonry buildings is generally based on a two-level approach, regarding local and global analyses (Pantò and Caliò 2022). Local analysis assesses all the possible out-of-plane (OOP) mechanisms of the building, while the global one focuses on the building box-type behaviour regarding in-plane (IP) wall failures. The analysis of OOP mechanisms is of fundamental importance especially for historic or old buildings or arch-type structures (Andreini et al. 2013; Ferreira et al. 2015), either not seismically designed or designed with

B. Pantò
University of Durham, Durham, UK

L. Giresini
Sapienza University of Rome, Rome, Italy

C. Casapulla (✉)
University of Naples Federico II, Naples, Italy
e-mail: casacla@unina.it

Published online: 01 October 2024

obsolete seismic standards. These modes are generally analysed by performing either force-based or displacement-based approaches (Sorrentino et al. 2017), using kinematic analyses (Casapulla and Argiento 2016; Chiozzi et al. 2019; Degli Abbati et al. 2021; Casapulla et al. 2021) or dynamic analyses (Giresini et al. 2021a; AlShawa et al. 2023; Coccia and Como 2023), as well as using computational homogenization methods (Addessi et al. 2017, 2021; D'Altri et al. 2020; Grillanda et al. 2020).

Regarding kinematic analyses of simple rocking walls, the basic model firstly proposed by Heyman (1966) was properly extended to include interlocking effects due to friction with the sidewalls, made of regular masonry with a running bond pattern, both at the onset (Casapulla 2001) and during the evolution of the rocking mechanism (Casapulla and Argiento 2016), through the implementation of the macro-block model (MBM). The related formulation for the frictional resistances was then adopted by the Italian seismic codes (MIT 2019) and the MBM was further extended to non-regular masonry patterns by Szabó et al. (2022) and by Funari et al. (2022).

As regards dynamic analyses, approaches considering rigid-block models connected to sidewalls, tie-rods, vaults, or energy dissipation devices were recently developed also including fragilities (Jaimes et al. 2021; Giresini 2022; Nale et al. 2023). Among these boundary conditions, it is confirmed that the most important ones are the sidewalls, due to the one-sided motion caused by their interlocking with rocking façades. Referring to rigid-block models, the role of sidewalls is considered by either assuming a modified coefficient of restitution (Sorrentino et al. 2011) or explicitly accounting for a rigid or elastic unilateral contact (Giresini et al. 2021b; Alshawa et al. 2023).

Nevertheless, the dynamics of rigid-block motion is affected by some limitations, as it neglects masonry deformability, three-dimensional wall boundary conditions and complex failure mechanisms other than simple overturning or horizontal/vertical bending. That is why more sophisticated approaches have been established making use of discrete macro-element (DMEM), distinct element (DEM) and detailed finite element (FEM) models. Among these, the DMEM is characterized by a very low computational cost compared to DEM and FEM, also with reference to geometrical consistency, possibility of combining discrete and finite elements, simple model calibration, possibility of use at macro and meso-scale (Vadalà et al. 2022). Recently, the DMEM was enriched by considering P-delta effects through a standard iterative Newton-Raphson method implemented in the commercial engineering-oriented HiStrA software package (Cusmano et al. 2023). The introduction of geometrical nonlinearities was validated through numerical and experimental results available in the literature, demonstrating its capability to describe the nonlinear response of rocking masonry walls subjected to different boundary and loading conditions.

However, apart from some micro/meso-scale implementations, especially with DEM (Chen and Bagi 2020; Pulatsu et al. 2022; Orosz and Bagi 2023) and FEM (Pepe et al. 2020; Yavartanoo and Kang 2022), interlocking effects of walls with adjacent sidewalls are still not properly simulated in the modelling approaches with low computational effort, like those on a macro scale (Casapulla et al. 2021). An original contribution in this line is the attempt to convert the analytical frictional resistances of the MBM proposed by Casapulla and Argiento (2016) into a spring bed distribution characterized by an equivalent tensile stiffness for the rocking response of a nonlinear dynamic model (Casapulla et al. 2017). Two potential approaches to define an equivalent tensile stiffness accounting for interlocking were discussed in that work, with reference to the nonlinear force-displacement curve: the first one consists in considering the ultimate displacement of the constant frictional resistance *plateau*, occurring between the activation of motion and the first loss of contact in the units, whilst the second one assumes a mean displacement value in the range of the subsequent decreasing frictional resistances, due to the progressive detachment of bed joints. However, the dynamic model only considered the elastic behaviour of the springs and neglected the evolution of the frictional resistances after the motion activation.

To contribute to research in this field, this paper presents an upgrade of the DMEM to assess the performance of rocking masonry walls also accounting for the frictional resistances exerted by the sidewalls. More specifically, the proposed modelling strategy implements the MBM analytical formulation, describing the interlocking mechanisms between the rocking front wall and the sidewalls, made of regular masonry with a running bond pattern, within the DMEM framework by means of a vertical distribution

of lateral elastic-plastic links (interlocking links). The ultimate forces and displacements of these links are properly calibrated to simulate the activation and the development of vertical cracks between the rocking wall and the sidewalls. To this aim, the original analytical representation of the frictional resistances of the MBM is converted into continuous variables, both at the onset and during the evolution of motion.

The two novelties of the paper, the continuous formulations for the frictional resistances in the MBM and the upgraded DMEM with a discrete distribution of interlocking links, allow an accurate seismic assessment of OOP loaded masonry walls, based on more realistic boundary conditions and a drastic reduction of the computational burden if compared to large displacement-finite element approaches.

The case of simple rocking of a front wall is only considered here, but the analysis can be easily extended to the compound rocking mechanism, generally involving triangular portions of the sidewalls, or to the corner failure relating to the external edges of buildings (Casapulla et al. 2019, 2021; Chiozzi et al. 2019; Grillanda et al. 2020).

After this introduction, the paper is organised as follows. Section 2 illustrates the frictional model (MBM) with its implications in a pushover analysis of a rocking façade and the definition of the continuous formulations allowing discretising the frictional resistances as a number of elastic-plastic springs with their own stiffness. Section 3 presents the implementation and calibration procedure of these springs within the DMEM strategy to describe the interaction between a masonry front wall and adjacent sidewalls. Section 4 discusses pushover analyses conducted on a front wall of a two-storey URM building available in the literature. The results predicted by the DMEM are finally compared to the analytical force-displacement curves obtained by the MBM and to those derived from the original source of the case study.

2 Simulation of the wall interlocking using the macro-block model

2.1 Continuous frictional interlocking formulations

The refined macro-block model (MBM) suitable for analysing local mechanisms in multi-storey URM buildings (Casapulla et al. 2021) is herein used to develop continuous formulations for the interlocking between orthogonal walls based on frictional resistances. Only the simple rocking-sliding mechanism of the front wall of a single-storey building under horizontal actions is considered here, with vertical cogged cracks close to the connections between the front wall and the sidewalls, as it is often observed in historic buildings due to the presence of weak connections between orthogonal walls (Fig. 1). In this figure, the directions Y-Z and X-Z identify the planes of the façade and the sidewalls, respectively.

According to the concept of macro-modelling, it is assumed that these cogged cracks, one per sidewall, divide the structure into two macro blocks (the moving front wall and the sidewalls which remain still), and all the possible relative motions among micro blocks (units) are concentrated along the interlocking links. Regular masonry units and staggering (single-leaf walls arranged in a running bond pattern) with infinite strength in compression, tension, and shear are assumed (Fig. 2a), while no-tension and frictional behaviour are considered at their contact interfaces along the cracks (Coulomb failure criterion). The latter assumption is used to simulate the interlocking between the front

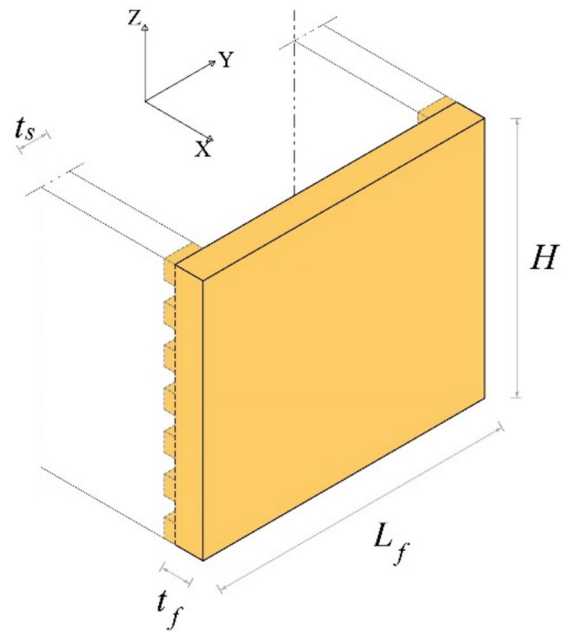

Fig. 1 MBM. 3D representation of the three-wall system composed of the front wall (highlighted in yellow) with some connections (still in yellow) with two sidewalls

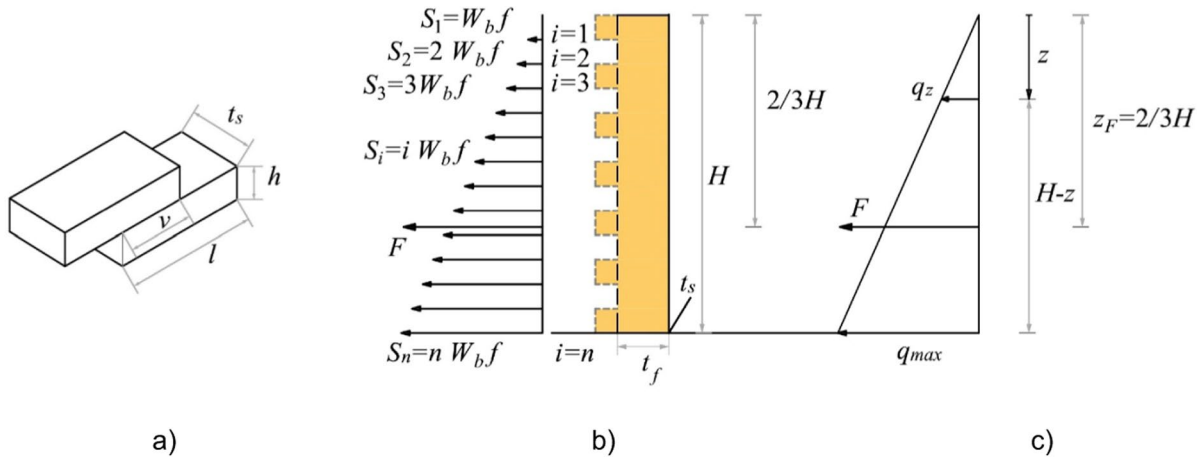

Fig. 2 MBM. **a** Masonry unit dimensions; **b** frictional resistances transmitted to the front wall (in yellow colour) by the sidewalls along the vertical cogged crack; **c** linear representation of the frictional resistances

and orthogonal walls based on frictional forces, as described by Casapulla (2001), and then adopted by the Commentary to the Italian technical standards, namely CNTC19 (MIT 2019), with a formulation of the resultant frictional resistance on each sidewall here rearranged as (Fig. 2b):

$$F = \sum_{1}^{n} S_i = \frac{n(n+1)}{2} v h t_s \gamma_s f = \frac{n(n+1)}{2} W_b f \tag{1}$$

In this equation, n is the number of courses in the sidewall crossed by the crack, γ_s is the specific weight of the sidewalls, f is the friction coefficient, and t_s, h and $v=l/2$ are the width (assumed equal to the sidewall thickness), height and overlapping length of the unit, respectively, as sketched in Fig. 2a. Note that W_b is the weight of a single half-unit (Fig. 2a and b) and CNTC19 suggests a reduction of F as expressed in Eq. (1) by 20% to account for rocking-sliding motion.

As shown in Fig. 2b, where t_f is the front wall thickness, the frictional forces at each bed joint linearly increase with the height of the sidewall top down, with the application point of their resultant (F) at 2/3 of the total height H from the top. Based on that, Eq. (1) can be expressed through the continuous variable q_z, being z the variable height from the top, as (Fig. 2c):

$$F = \int_0^H q_z d_z = \frac{H\, q_{max}}{2} \tag{2}$$

from which, known F, q_z and the application point of its resultant, z_F, can be derived as follows:

$$\begin{aligned} q_z &= \frac{z}{H} q_{max} = \frac{2F}{H^2} z \\ z_F &= \frac{\int_0^H (q_z z d_z)}{F} = \frac{2}{3} H \end{aligned} \tag{3}$$

The continuous formulations in Eq. (3) allow discretising the frictional resistances as a number of elastic-plastic springs with their own stiffness, as described in Sect. 3.

3 Incremental limit analysis for the simple rocking-sliding mechanism of masonry walls

The simple rocking failure of the front wall is a mechanism not involving portions of the sidewalls and its crack pattern is identified a priori. In fact, only the front wall is involved in the mechanism when it starts rotating around its external bottom edge (ideally a cylindrical hinge) and vertical cracks occur along the intersections with the sidewalls. In case of some interlocking of the front wall with the sidewalls, it is assumed that the cracks are still vertical but with a cogged shape due to the projection of the interlocked masonry units (Fig. 2b), which involves a clear prevalence of sliding along the bed joints during the motion. In this case, examined in detail in the following, the simple rocking can be defined as a rocking-sliding mechanism.

The evolution of this mechanism after the formation of the hinge strictly depends on the frictional

forces, which gradually decrease after a certain displacement, due to the progressive loss of contact between the units along the cracks. The variation of these forces can be represented by nonlinear (step-type) functions of the horizontal displacement, as originally developed within the MBM by Casapulla and Argiento (2016) and briefly recalled in the following.

The effectiveness of these forces calculated by Eq. (1) on the whole height H of each sidewall is guaranteed as long as the first two courses on top lose their contact with the fixed portion of the wall along the crack (first threshold displacement). As the wall rotation increases, the subsequent threshold displacements are assumed to be attained at every two underlying courses of the front wall that lose the contact with the sidewall. This means that, considering the generic detached course i in Fig. 3, the threshold horizontal displacement is reached when $dx_i = v$, i.e. when the overlapping of units is lost at the distance from the base equal to $(r_i \bullet h)$, being $r_i = n - i (i = 0, 2, 4, \ldots, n)$ the number of courses still involved in frictional contact and h the unit height. At the same step, the displacement of the front wall centroid (dx_{Gi}) with a generic position (x_G, z_G), reads:

$$dx_G = \frac{nv}{2r_i} \tag{4}$$

while the corresponding reduced frictional resistance F_i can be easily calculated by replacing n with r_i, in Eq. (1), i.e.:

$$F_i = \frac{r_i(r_i+1)}{2} W_b f \tag{5}$$

Then, nonlinear kinematic analysis allows investigating the evolution of the mechanism until the collapse through a pushover curve, which relates the horizontal load F_h to the horizontal displacement of the front wall centroid dx_G (Fig. 3), assumed as the control point. The curve can be obtained by applying the theorem of virtual works, considering varied kinematic configurations of the examined mechanism at large displacements, as (Fig. 4):

$$F_h(\vartheta) = \frac{W x_G(\vartheta) + 2F_i z_F(\vartheta)}{z_G(\vartheta)} \tag{6}$$

where ϑ is the wall finite rotation, while the horizontal displacement of the control point reads:

$$dx_G(\vartheta) = \frac{t_f}{2} - x_G(\vartheta) \tag{7}$$

It is worth noting that F_i in Eq. (6) follows the variability of Eq. (5) and that at the onset of the mechanism ($\vartheta = 0$) F_h has its maximum value, as sketched for the pushover curves developed for the case study in Sect. 4.

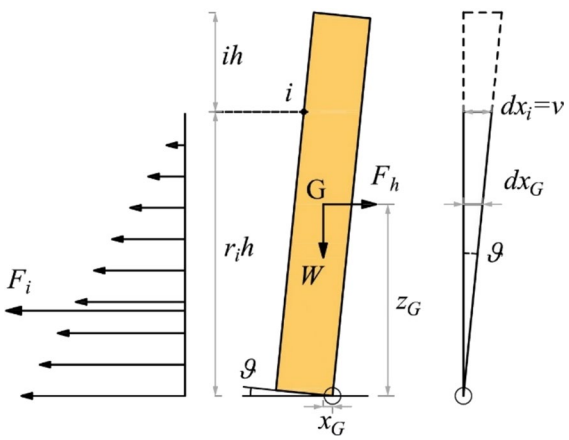

Fig. 3 MBM: variation of frictional resistances at increasing wall rotation

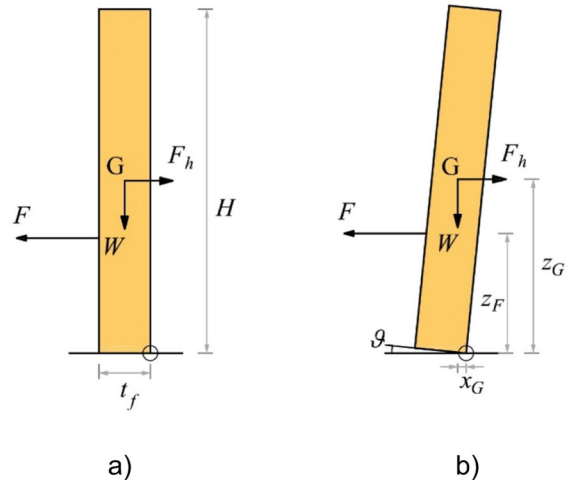

Fig. 4 MBM: **a** Initial and **b** varied kinematic configurations of the rocking front wall

4 Implementation within the macro-element model

The discrete macro-element model (DMEM) strategy consists in discretising a masonry wall with a mesh of shear-deformable spatial macro-elements (Fig. 5) connected to the other elements through nonlinear zero-thickness interfaces (Fig. 5b). Each macro-element is characterised by seven degrees of freedom describing the six independent rigid displacements (U, V, W, Φ, Θ, Ψ) of the element and one parameter (g) representing the element shear deformation. Each interface comprises a set of nonlinear mono-dimensional links calibrated by performing straightforward equivalences between the continuum material and the equivalent discrete model (Pantò et al. 2017; Chácara et al. 2019).

The number of orthogonal links is generally chosen according to the desired level of accuracy to attain for the interface integration. It is worth noting that no additional Lagrangian parameters are needed to describe the kinematics of interfaces. More details on the model formulation and validation can be found in Caliò et al. (2012) and in Pantò et al. (2017).

The links describing the sliding at the base interface of the front wall are kept elastic and sufficiently rigid, while the base vertical links, governing the base partialisation of the wall, are considered elastic in compression and with zero tensile strength. According to Cusmano et al. (2023), the interface at the base of the front wall can be discretised in 20 rows of vertical links along the wall OOP direction. It has been proven that this degree of discretisation guarantees a high level of accuracy in simulating the progressive partialisation of the wall base, in order to ensure a good agreement with the hypothesis of rigid body overturning around the wall vertex assumed by the MBM.

The DMEM P-Delta formulation recently proposed by Cusmano et al. (2023) is here employed to perform the analyses. According to it, the geometrical nonlinearities are considered by updating the current positions of the external and along-interface internal forces applied to the macro-elements. Such a simplified procedure avoids assembling and updating the geometrical stiffness matrix according to the current system configuration, ensuring a good model efficiency.

5 Interlocking links

Based on the frictional model (MBM) illustrated in Sect. 2, the interaction between the masonry front wall and each sidewall is here implemented within the DMEM strategy through a discrete lateral distribution of 1D nonlinear links, herein called 'interlocking links', each describing the interaction among a number of courses (for example, an interlocking link simulating two courses is sketched in Fig. 6a). The mechanical behaviour of each of these links is nonlinear and characterised by an initial stiffness K, an ultimate force F_u, and an ultimate displacement d_u, at which the strength of the links drops to zero, as displayed in Fig. 6d. The ultimate force of the generic j-th link is expressed as:

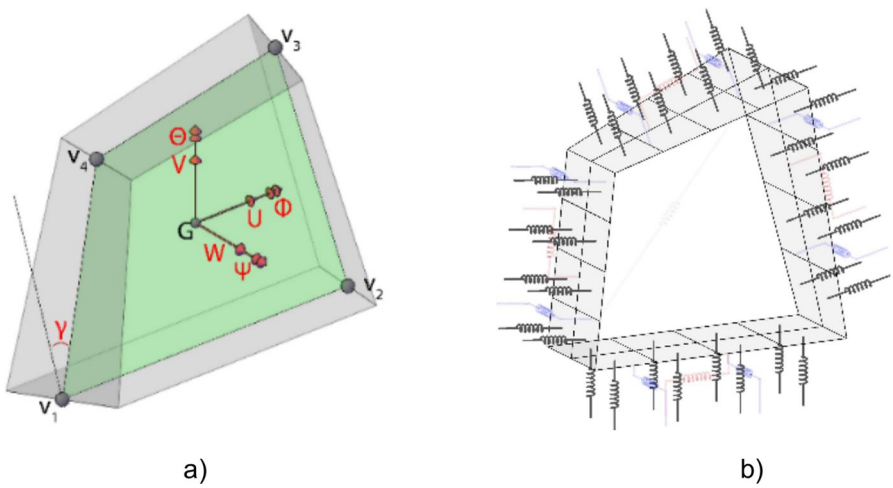

Fig. 5 DMEM: **a** Lagrangian parameters of the macro-element; **b** interface nonlinear links

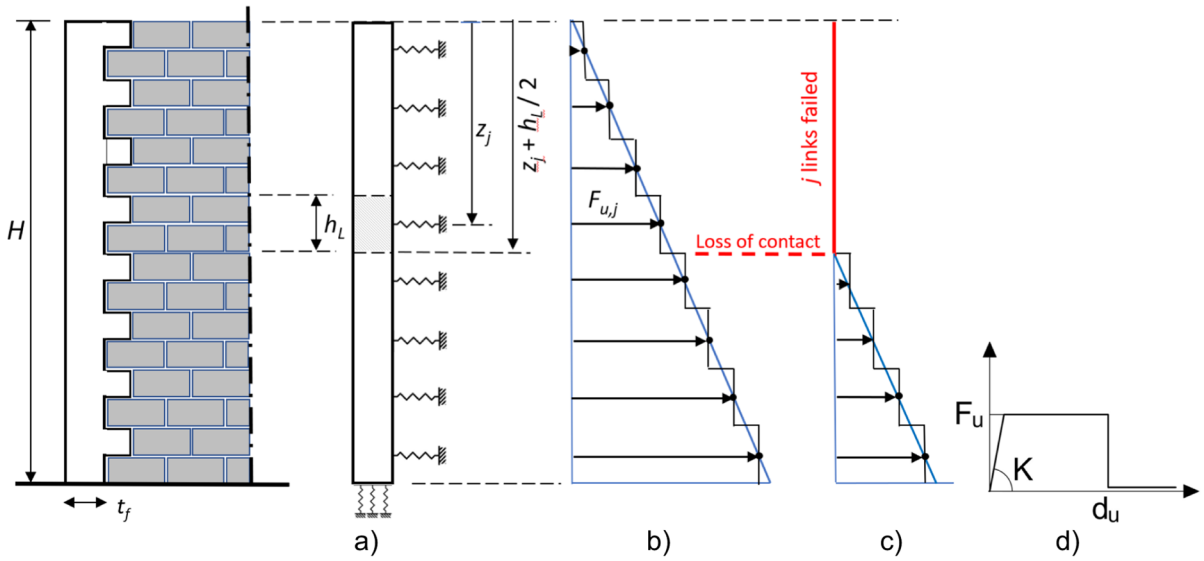

Fig. 6 DMEM. **a** Typological regular interlocking between the front wall and sidewalls and its numerical simulation by 1D discrete link distribution; overlapping of the frictional resistance distributions for the DMEM (black stepped line) and the MBM (blue straight line) in the cases of **b** all links active and **c** loss of contact at the first j links; **d** constitutive law of each nonlinear link

$$F_{u,j} = q_{z,j} h_L \tag{8}$$

where $q_{z,\,j}$ is the distributed frictional force per unit length at z_j, given by the first of Eq. (3), and h_L is the link tributary height, coincident with the link-to-link distance (Fig. 6a). The equivalence between the continuous function of the frictional resistances in Fig. 2c (expressed by Eq. (1)) and their discrete variation (provided by Eq. (8)) is displayed in Fig. 6b, where the linear and the stepped functions are overlapped. The ultimate displacement $d_{u,j}$ of the generic j-th interlocking link is associated with the loss of contact at the bottom section of the tributary height represented by the link, whose distance from the top of the wall can be expressed as $z_j + h_{L/2}$. It results:

$$d_{u,j} = \frac{l}{2} \frac{H - z_j}{H - \left(z_j + \frac{h_L}{2}\right)} \tag{9}$$

where l is the unit width (Fig. 2a). Finally, the elastic stiffness K is evaluated considering a displacement of 0.1 mm when the link attains the ultimate force. This value is arbitrarily assumed to simulate a quasi-rigid behaviour of the interlocking link before the activation of sliding.

6 Pushover analysis

The pushover analyses employing the DMEM approach are carried out by considering an incremental process where the external load F_h is applied to the front wall centroid. At each analysis step, the stiffness matrix and the load vector are updated to take into account the nonlinearities of the interface links and the geometrical nonlinearities (P-Delta effects). At each step, the equilibrium is reached by an iterative Newton-Raphson procedure with an arch-length control method to follow the softening branch of the capacity curve (Pantò et al. 2017; Cusmano et al. 2023).

The wall section partialisation starts when the first row of the vertical links of the interface at the wall base goes in tension and progresses until only one row remains in compression. This corresponds to the activation of the rocking mechanism, characterised by the rotation of the front wall around a cylindrical hinge at the active row of vertical links,

which is not at the external edge, as assumed in the MBM, but very close to it.

Concerning the frictional resistances, in the stage when all the interlocking links are active ($d_j \leq d_{u,j}$), the resistant forces of these links approximate the triangular distribution of the continuous variables, as shown in Fig. 6b, where the black stepped line indicates the forces corresponding to the links of the DMEM and the blue straight line is the force distribution corresponding to the MBM. Finally, the force of each interlocking link drops to zero when the link attains the ultimate displacement, and the force of the link is redistributed to the other links, as represented by the MBM in Figs. 3 and 6c. In fact, the stabilising weight of the masonry "column" above each considered sliding interface is updated in the DMEM at the end of each analysis step accounting for the failure of each link. The current forces of the links are evaluated by applying Eq. (8), where the total force ($2F$) is updated considering the current effective wall height, excluding the wall portion corresponding to the failed links. As a result, the DMEM links provide the discrete distribution that perfectly approaches the triangular force distribution of the MBM, with zero at the sliding surface of the lowest failed interlocking link, as illustrated in Fig. 6c representing the case of the first j top links failed.

6.1 Results and discussions

This section illustrates and compares the results obtained by the DMEM and MBM approaches applied to a selected case study. This is represented by a two-storey URM building, considered as a benchmark study within the Italian ReLUIS III research project on Masonry Structures (Cattari and Magenes 2021), which was mostly investigated with regard to its global behaviour rather than to local failure modes (Fig. 7a). In particular, the front wall of this building, assumed without openings, was analysed by Galvez et al. (2021) with reference to its OOP behaviour, using the discrete element modelling (DEM) approach to simulate the interlocking with two sidewalls (Fig. 7b). This peculiar analysis makes this case study the most suitable one currently available in the literature for its direct comparison with the approaches proposed here. It is worth highlighting that this is also the reason why the openings are still neglected in these analyses, even if considering them would only imply a reduction in the specific weight of the front wall and a slight shift of its centroid, changes that are very simple to implement.

The elements representing the interlocking between the front and the sidewalls are 20 courses of bricks with adapted dimensions of $0.250 \times 0.322 \times 0.375$ m^3 ($l \times h \times t_s$), arranged in a running bond pattern, while

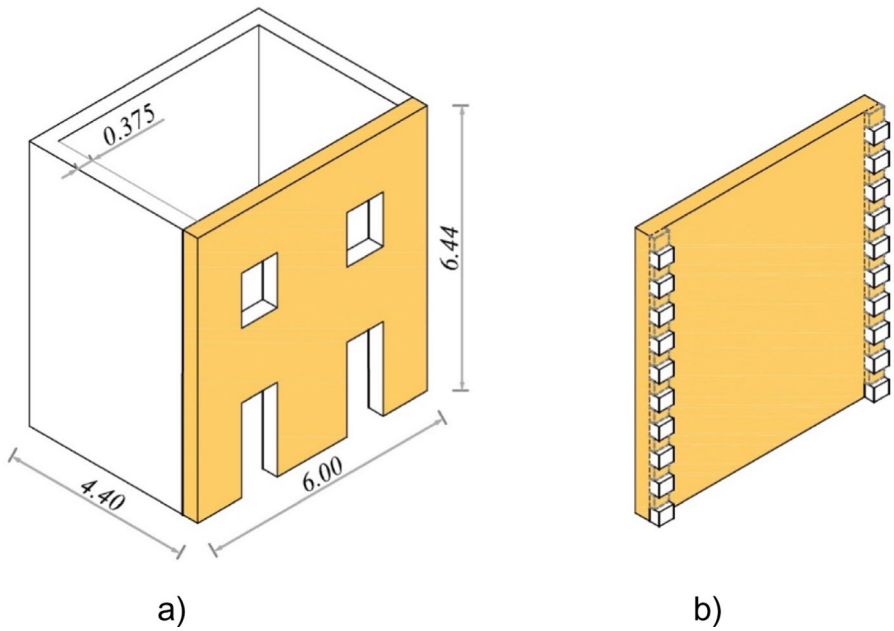

Fig. 7 Geometrical model of the case study building. **a** Units in m; **b** front wall without openings but with interlocking with the sidewalls

the friction coefficient is assumed to be $f = 0.577$ and the frictional resistances are reduced by 20% according to CNTC19 (MIT 2019).

Using the MBM with Eqs. (5) and (6), the frictional resistance-displacement curve referred to the control point of the front wall (i.e. its centroid) and to the contribution of both sidewalls (i.e. to $2F$) is reported as a continuous red line in Fig. 8a. It highlights the drop of frictional resistance as the wall rotation increases after the first threshold displacement (dx_G = 0.07 m in this case) and the residual resistance kept as the control point reaches the ultimate displacement (dx_G = 0.1875 m), assumed as half the thickness of the front wall. The related pushover curve according to Eqs. (6) and (7) is displayed in Fig. 8b, together with the case of the isolated front wall (no interlocking), represented by the grey continuous line. In particular, the first linear descending branch of the red pushover curve is characterised by the effectiveness of frictional resistances acting on the whole height of the wall intersections, till when these values start to decrease in correspondence with the first threshold displacement given by Eq. (4) with $i = 2$. Considering the effective vertical cracks at the wall intersection, the subsequent nonlinear reduction of frictional forces represented by Eq. (5) implies a linear descending stepwise function of F_h, with different measures of the risers and treads. In fact, it is worth noting that the increasing displacement of the control point involves longer descending branches and shorter step heights due to the higher displacement capacity associated with the lower part of the

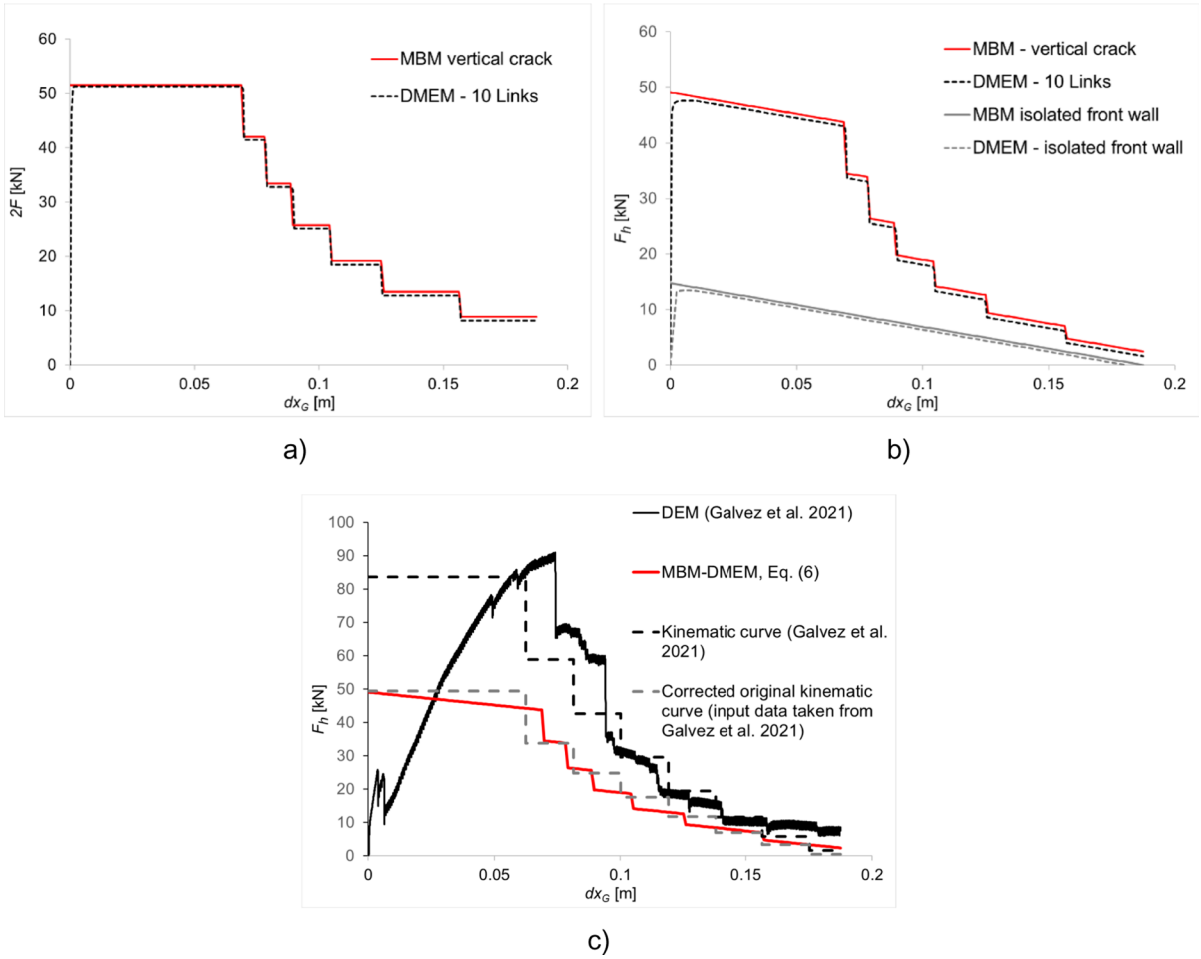

Fig. 8 **a** Frictional resistance-displacement curves and **b** pushover curves with reference to the front wall centroid and the contribution of both sidewalls; **c** comparisons of the MBM-DMEM pushover curves with those obtained by Galvez et al. (2021)

walls with respect to the upper one and lower frictional resistances, respectively, as better discussed by Casapulla and Argiento (2016).

Using the DMEM, different discretisation settings are adopted for the interlocking links: ten links (one link every two brick courses), five links (one link every four brick courses), two models with a reduced number of links (3 and 2), and finally a model with a single link proposed as a limit case. The calibration of the strengths and the application points of the links belonging to any distribution must follow the equivalence with the continuous distribution of the MBM (Fig. 2c), in terms of both resultant force and moment. So, as introduced above, each link is located at the centroid of the link tributary height h_L, as displayed in Fig. 6a, and the link ultimate displacement is evaluated considering the sliding section coincident with the bottom section of the link height. When a single link is adopted, it is located at 1/3 of the height from the base to guarantee the same ultimate moment of the analytical MBM, and the link ultimate displacement is conventionally evaluated considering the sliding section at 2/3H.

The results of the link calibration are summarised in Table 1, where the first two columns after the j column represent the abscissas of the j-th link position and the corresponding sliding surface (controlling the loss of contact for the link), respectively. The fourth and fifth columns report the ultimate force and displacement of the link calculated by using Eq. (8) and Eq. (9), respectively, and finally, the last column reports the elastic stiffness evaluated upon the ultimate force and the yield displacement empirically assumed equal to 0.1 mm.

The results of the analyses considering 10 interlocking links are shown in Fig. 8, comparing the MBM and the upgraded DMEM in terms of frictional resistances by both sidewalls (Fig. 8a), and external force (Fig. 8b) vs. the front wall centroid. The results for the isolated wall are also reported in Fig. 8b for comparison to highlight the significant role of the frictional resistances.

It can be easily observed that the results predicted by the two models are practically coincident (Fig. 8a and b) and represent the failure of 6 out of 10 interlocking links. Instead, some differences can be noted against the two curves obtained by Galvez et al. (2021) in Fig. 8c, one (black dashed curve) derived using limit analysis and the other (black continuous curve) using the DEM approach. In fact, these results are mostly affected by an overestimation of the horizontal load in the kinematic curve at the activation of motion with respect to Eq. (6), represented by the red curve, also influencing the subsequent capacity reductions at large displacements. A personal communication with the authors of that paper clarified that this overestimation is basically due to the doubling of the frictional resistances, derived from the assumption of the weight W_b of the single half-unit in Eq. (1) as if it were a whole unit. By correcting values given in the original publication, the horizontal load F_h at J=0, calculated with Eq. (6), would shift from 84 kN to 49 kN and the new grey dotted pushover curve could be derived for the kinematic curve of Galvez et al. (2021). Apart from some approximations in the shape of risers and treads within this corrected step function of F_h, the recalibrated DEM curve is also expected to have a similar trend in terms of displacements during wall separation, meaning that all the curves would be very close to each other if the mentioned overestimation were removed.

Finally, a parametric analysis is developed by varying the number of the interlocking links disposed along with the wall height, calibrated as previously explained. The results, shown in Fig. 9, evidence that the models with ten, five and three links provide very similar predictions in terms of peak horizontal force (Fig. 9b), ranging from 47.6 kN (predicted by the model with ten Links) and 49.3 kN (predicted by the model with three Links), with a difference of 3.6% comparing the model with three links to the most refined one with ten links. The discrepancy increases to 8.6%, considering the model with two links, which predicts a peak horizontal force of 51.7 kN. Moreover, as expected, the DMEM tends to overestimate the horizontal displacement capacity of the system while reducing the number of links. Namely, the first drop of the horizontal force F_h is predicted at 0.07 m by the model with ten links and at 0.08 m, 0.094 m, and 0.125 m by the models with five, three, and two links, respectively (Fig. 9a, b). Finally, with respect to the results of the MBM and the 10-Link DMEM, the model with a single link guarantees an excellent prediction of the response of the system up to the lateral displacement of 0.07 m, approximately 40% of the critical displacement. After this displacement, it overestimates the horizontal force of the system up to the displacement of about 0.09 m, approximately 50%

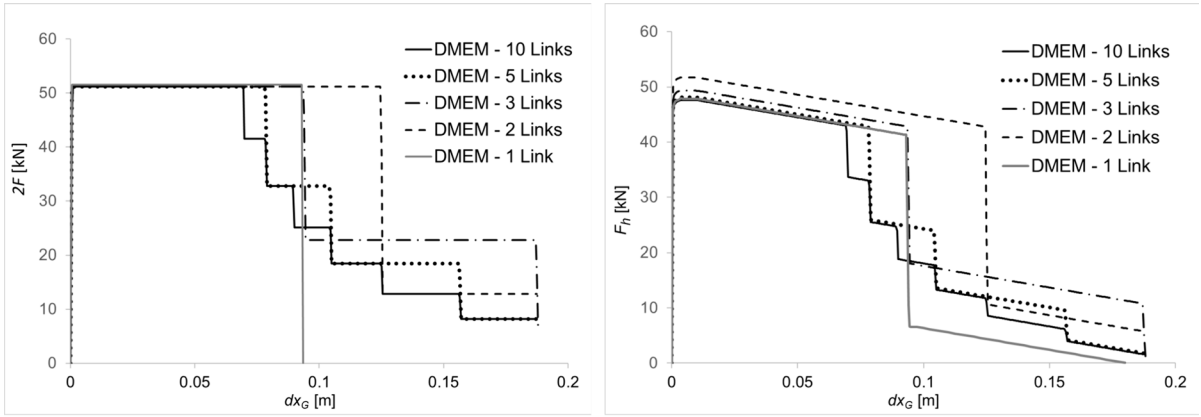

Fig. 9 DMEM. **a** Frictional resistance-displacement curves and **b** pushover curves for different link discretisation settings

Table 1 Calibration of the DMEM links

j	z_j	$z_j + 0.5h_L$	$F_{u,j}$	$d_{u,j}$	K_j
	m	m	kN	m	kN/m
10 links					
1	0.32	0.65	0.26	0.132	2576
2	0.97	1.30	0.77	0.133	7728
3	1.62	1.94	1.29	0.134	12880
4	2.27	2.59	1.80	0.135	18032
5	2.92	3.24	2.32	0.138	23184
6	3.56	3.89	2.83	0.141	28344
7	4.21	4.54	3.35	0.146	33496
8	4.86	5.18	3.86	0.156	38648
9	5.51	5.83	4.38	0.188	43800
10	6.16	6.48	4.90	-	48952
5 links					
1	0.65	1.30	1.03	0.141	10304
2	1.94	2.59	3.09	0.146	30920
3	3.24	3.89	5.15	0.156	51528
4	4.54	5.18	7.21	0.188	72136
5	5.83	6.48	9.28	-	92752
3 links					
1	1.08	2.16	2.86	0.156	28624
2	3.24	4.32	8.59	0.188	85880
3	5.40	6.48	14.31	-	143136
2 links					
1	1.62	3.24	6.44	0.188	64408
2	4.86	6.48	19.32	-	193232
1 link					
1	4.32	3.24	25.76	0.094	257640

of the critical displacement, at which it predicts 41 kN for the horizontal force against 18 kN evaluated by the 10-link DMEM. Comparing the 3-Link and the single-link DMEMs, it is worth noting that *i*) they provide equivalent responses up to 50% of the critical displacements, where the two models register almost contemporarily the drop of the force (the top control sliding surface of the 3-Link DMEM coincides with the sliding surface of the 1-Link DMEM); *ii*) the single-link DMEM provides a safe prediction in the range of $dx_G > 50\%$ of the critical displacement; conversely, the 3-Link DMEM overestimates the effective horizontal force of the system.

The above-described comparisons demonstrate that the single-link DMEM is a promising and efficient tool for practical applications and assessments, for which the limit of 40% is identified as the threshold of the ultimate performance level by CNTC19 (MIT, 2019).

7 Conclusion

The paper presents a new implementation within the discrete macro-element method (DMEM) to describe the interaction between rocking masonry walls and adjacent sidewalls. These interlocking effects are simulated through frictional resistances whose distribution follows the analytical formulation developed for the macro-block model (MBM) in turn used for macro-limit analysis. Based on the

equivalence of the continuous distribution of these forces and the discrete distribution of lateral elastic-plastic links, an upgraded DMEM is developed to simulate the onset of the rocking-sliding mechanism and its evolution, even exploiting a recently proposed P-Delta DMEM formulation. The model accuracy is evaluated considering a case study extracted from the literature by performing pushover analyses and comparing the results against those obtained by the MBM, both in terms of frictional forces and pushover capacity curves. The results evidence a good consistency between the DMEM and the MBM, confirming that the upgraded model represents an effective numerical tool capable of developing accurate seismic assessments of OOP loaded masonry walls and monumental façades, with a drastic reduction of the computational burden if compared to large displacement-finite element approaches.

Moreover, the influence of the number of interlocking links on the wall response is investigated. The results of parametric analyses show the capability of the DMEM in employing a single link to simulate the response of the wall until a limit of approximately 40% of the critical displacement, making this simplified model suitable to be employed for practical assessments of masonry walls subjected to rocking failure mechanisms.

At this stage, the DMEM is developed by considering a single macro-element to make comparisons with the MBM in a more straightforward way, also considering the mechanical complexity of the interlocking effect. Further investigations considering a mesh discretisation of the front wall as well as dynamic approaches, allowing for simulating wall openings and more complex failure mechanisms, will be the object of future works.

Author contributions B.P., L.G. and C.C. have contributed equally to this work.

Funding Open access funding provided by Università degli Studi di Napoli Federico II within the CRUI-CARE Agreement. This research was partially financed by Sapienza University of Rome, within the project "ANalytical Unified Modelling of A New earthquake-resistant device for the reduction of seismic vulnerability of masonry buildings (ANUMAN)" no. protocol RP1221814E212601.

Data availability No datasets were generated or analysed during the current study.

Declarations

Conflict of interest The authors declare no competing interests.

Ethical approval Not applicable.

References

Addessi D, Di Re P, Gatta C, Sacco E (2021) Multiscale analysis of out-of-plane masonry elements using different structural models at macro and microscale. Comput Struct 247:106477

Andreini M, De Falco A, Giresini L, Sassu M (2013) Structural analysis and consolidation strategy of the historic Mediceo Aqueduct in Pisa (Italy). Appl Mech Mater 351–352:1354–1357

Caliò I, Marletta M, Pantò B (2012) A new discrete element model for the evaluation of the seismic behaviour of unreinforced masonry buildings. Eng Struct 40:327–338

Casapulla C (2001) Dry rigid block masonry: safe solutions in presence of Coulomb friction. WIT Trans Built Environ 55:251–261

Casapulla C, Argiento LU (2016) The comparative role of friction in local out-of-plane mechanisms of masonry buildings. Pushover analysis and experimental investigation. Eng Struct 126:158–173

Casapulla C, Giresini L, Argiento LU, Maione A (2019) Non-linear static and dynamic analysis of rocking masonry corners using rigid macro-block modelling. Int J Struct Stabil Dynam 19(11):1950137

Casapulla C, Argiento LU, Maione A, Speranza E (2021) Upgraded formulations for the onset of local mechanisms in multi-storey masonry buildings using limit analysis. Structures 31:380–394

Cattari S, Magenes G (2021) Benchmarking the software packages to model and assess the seismic response of URM existing buildings through nonlinear analyses. Bull Earthq Eng 20:1901–1936

Chácara C, Cannizzaro F, Pantò B, Caliò I, Lourenço PB (2019) Seismic vulnerability of URM structures based on a discrete macro-element modeling (DMEM) approach. Eng Struct 201:109715

Chen S, Bagi K (2020) Crosswise tensile resistance of masonry patterns due to contact friction, proceedings of the royal society a: mathematical,. Phys Eng Sci 476:20200439

Chiozzi A, Grillanda N, Milani G, Tralli A (2019) NURBS-based kinematic limit analysis of FRP-reinforced masonry walls with out-of-plane loading. Frattura Ed Integrità Strutturale 14(51):9–23

Coccia S, Como M (2023) Out-of-plane dynamical strength of masonry walls under seismic actions. J Earthquake Eng. https://doi.org/10.1080/13632469.2023.2228913

Cusmano V, Pantò B, Rapicavoli D, Caliò I (2023) A discrete-element approach accounting for P-Delta effects. Earthquake Eng Struct Dynam 52:2047–2066

D'Altri AM, Sarhosis V, Milani G, Rots J, Cattari S, Lagomarsino S, Sacco E, Tralli A, Castellazzi G, de Miranda S (2020) Modeling strategies for the computational analysis of unreinforced masonry structures: review and classification. Arch Comput Methods Eng 27(4):1153–1185

Degli Abbati S, Cattari S, Lagomarsino S (2021) Validation of displacement-based procedures for rocking assessment of cantilever masonry elements. Structures 33:3397–3416

Ferreira TM, Costa AA, Costa A (2015) Analysis of the out-of-plane seismic behavior of unreinforced masonry: a literature review. Int J Architectural Herit 9(8):949–972

Funari MF, Pulatsu B, Szabó S, Lourenço PB (2022) A solution for the frictional resistance in macro-block limit analysis of non-periodic masonry. Structures 43:847–859

Galvez F, Sorrentino L, Dizhur D, Ingham JM (2021) Using DEM to investigate boundary conditions for rocking URM façades subjected to earthquake motion. J Struct Eng, 147(11):04021191

Giresini L (2022) Effect of dampers on the seismic performance of masonry walls assessed through fragility and demand hazard curves, Eng Struct 261:114295

Giresini L, Casapulla C, Croce P (2021aaa) Environmental and economic impact of retrofitting techniques to prevent out-of-plane failure modes of unreinforced masonry buildings. Sustainability, 13(20):11383

Giresini L, Taddei F, Solarino F, Mueller G, Croce P (2021bb) Influence of stiffness and damping parameters of passive seismic control devices in one-sided rocking of masonry walls. J Struct Eng (ASCE), 148(2):04021257

Grillanda N, Valente M, Milani G, Chiozzi A, Tralli A (2020) Advanced numerical strategies for seismic assessment of historical masonry aggregates. Eng Struct, 212:110441

Heyman J (1966) The stone skeleton. Int J Solids Struct 2(2):249–279

Jaimes MA, Chávez MM, Peña F, Garcia Soto A (2021) Out-of-plane mechanism in the seismic risk of masonry façades. Bull Earthq Eng 19:1509–1535

Nale M, Benvenuti E, Chiozzi A, Minghini F, Tralli A (2023) Effect of uncertainties on seismic fragility for out-of-plane collapse of unreinforced masonry walls. J Build Eng, 75:106936

Orosz Á, Bagi K (2023) Comparison of contact treatment methods for rigid polyhedral discrete element models, Int J Rock Mech Mining Sci, 170:105550

Pantò B, Cannizzaro F, Caliò I, Lourenço PB (2017) Numerical and experimental validation of a 3D macro-model for the in-plane and out-of-plane behavior of unreinforced masonry walls. Int J Architectural Herit 11(7):946–964

Pepe M, Pingaro M, Trovalusci P, Reccia E, Leonetti L (2020) Micromodels for the in-plane failure analysis of masonry walls: limit analysis, FEM and FEM/DEM approaches. Frattura ed Integrità Strutturale 14(51):504–516

Pulatsu B, Gencer F, Erdogmus E (2022) Study of the effect of construction techniques on the seismic capacity of ancient dry-joint masonry towers through DEM. Eur J Environ Civil Eng 26(9):3913–3930

Sorrentino L, AlShawa O, Decanini LD (2011) The relevance of energy damping in unreinforced masonry rocking mechanisms. Experimental and analytic investigations. Bull Earthq Eng 9:1617–1642

Sorrentino L, D'Ayala D, de Felice G, Griffith MC, Lagomarsino S, Magenes G (2017) Review of out-of-plane seismic assessment techniques applied to existing masonry buildings. Int J Architectural Herit 11(1):2–21

Szabó S, Funari MF, Pulatsu B, Lourenço PB (2022) Lateral capacity of URM walls: a parametric study using macro and micro limit analysis predictions. Applied Sciences, 12(21):10834

Vadalà F, Cusmano V, Funari MF, Caliò I, Lourenço PB (2022) On the use of a mesoscale masonry pattern representation in discrete macroelement approach. Journal of Building Engineering 50:104182

Yavartanoo F, Kang TH-K (2022) Dry-stack masonry wall modeling using finite-element method. J Struct Eng (ASCE) 148(11):04022176

Casapulla C, Giresini L, Argiento LU, Lagomarsino S (2017) Analisi statiche e dinamiche incrementali per la valutazione della risposta fuori piano della facciata di una chiesa colpita dal terremoto centro-Italia 2016-17,. Proceedings of the XVII ANIDIS Conference on L'Ingegneria sismica in Italia, Pistoia, Italy [in Italian]

Pantò B, Caliò I (2022) *Numerical modeling for the seismic assessment of masonry structures*. In: Seismic Vulnerability Assessment of Civil Engineering Structures At Multiple Scales, Woodhead Publishing, pp. 85–126

Addessi D Sacco, E Di Re P (2017) A micro-macro homogenization for modeling the masonry out-of-plane response, AIMETA 2017 - Proceedings of the 23rd conference of the italian association of theoretical and applied mechanics, 2: 1502–1514

Ministero delle Infrastrutture e dei Trasporti – MIT (2019) CNTC19-Circolare applicativa delle Norme Tecniche delle Costruzioni di cui al D.M. 17/01/2018 (NTC 2018). Gazzetta Ufficiale N. 42 del 20/02/2018. (in Italian)